Characterization of MoO$_X$ species on γ-Al$_2$O$_3$, Y and ZSM-5 zeolites during thermally activated solid–solid synthesis

Characterization of MoO$_x$ species on γ-Al$_2$O$_3$, Y and ZSM-5 zeolites during thermally activated solid–solid synthesis

Lourdes Mosqueira[1], Sergio A Gómez[2] and Gustavo A Fuentes[2]

[1] Programa de Ingeniería Molecular, Instituto Mexicano del Petróleo, 07730 México, DF, Mexico
[2] Departamento de Ingeniería de Procesos e Hidráulica, Universidad Autónoma Metropolitana-Iztapalapa, AP 55-534, 09340 México, DF, Mexico

E-mail: mmosquei@imp.mx

Abstract

We characterized the Mo surface species present during thermally activated solid–solid synthesis of Mo/γ-Al$_2$O$_3$, Mo/H-ZY and Mo/H-ZSM-5 starting from mixtures of MoO$_3$ with γ-Al$_2$O$_3$ or zeolites H-Y and H-ZSM-5. We identified different surface molybdate species by using diffuse reflectance measurements in the UV–vis region and a bandgap analysis of the deconvoluted spectra. Species assignments were confirmed via theoretical DFT calculations of simplified zeolite clusters containing MoO$_x$ species as well as by analysis of the spectra of pure standards.

Migration of MoO$_x$ onto H-Y and H-ZSM-5 zeolites resulted in an important fraction of tetrahedral Mo species (monomers and dimers). On the other hand, migration on γ-Al$_2$O$_3$ led to the presence of a larger fraction of octahedral Mo oligomeric species. The variation in surface structures seems to be a function of the Si/Al ratio and of the pore structure of supports. Our results are consistent with a mechanism involving formation and migration of monomers and dimers (equivalent to [MoO$_4$]$^{2-}$ and [Mo$_2$O$_7$]$^{2-}$) leading to the formation of oligomers (resembling [Mo$_7$O$_{24}$]$^{6-}$). We present a simplified kinetic scheme for the formation of the different Mo compounds consistent with the characterization results.

1. Introduction

Molybdenum oxide-based materials are important as aromatization catalysts and also as intermediates during the synthesis of hydrotreating catalysts [1–3]. In order to be efficient, molybdenum has to be highly dispersed inside the porous structure of the support. In zeolites, the direct incorporation of well-defined MoO$_x$ species is difficult to achieve by classic methods

such as ionic exchange from an ammonium heptamolybdate solution [4, 5]. Alternatives have been proposed, such as aqueous ionic exchange of $[MoO_2]^{2+}$ [6] or $Mo_2(en)_4^{4+}$ [7], vapour phase adsorption of $MoCl_5$ [8] or $Mo(CO)_6$ [9, 10], direct incorporation of the active phase in the structure during zeolite synthesis [11], and the introduction of moieties via solid-state interactions, like ionic exchange in $MoCl_5$/zeolite-Y [12] and synthesis of MoO_3/H-ZSM-5 [13]. The last methods involve interactions between solid phases and comprise grinding, mixing and solid-on-solid wetting, which is usually induced by thermal activation [13, 14].

The thermal activation of solid-on-solid migration is different from the traditional solid-state synthesis insofar as the migration processes occur at the surface of one of the solids (the support) rather than through its lattice. Another difference has to do with the fact that the final material is composed of the support covered to different extents by moieties originating from the second solid. This is in contrast with the solid-state methods where the final material has a global structure different from the starting solids and only in the case of doping is the structure of the main material maintained. As a result of those differences the term solid–solid synthesis is used to refer to this method. The solid–solid synthesis of Mo-based catalytic materials has been performed since the 1970s. This method is simple and convenient because the final materials attain significant dispersions of Mo species, which makes them useful for catalytic applications. In recent years, the interest in synthesis via solid–solid methods has increased. In general, these methods involve the spreading of surface species derived from metal oxides with low Tammann temperatures, such as MoO_3, on refractory supports, i.e. γ-Al_2O_3 and zeolites.

Analysis of the processes occurring during direct solid–solid synthesis are relevant because they coincide with different steps of the conventional methods of synthesis, of processes involved in thermal deactivation, as well as during the different high-temperature calcination steps employed in the reactivation and rejuvenation of catalysts. Those processes determine the structure and morphology of active phases and therefore have an effect on their catalytic properties.

In spite of the number of studies made about solid–solid synthesis, it has been difficult to determine unequivocally the structure and amount of the different surface oxide species present. These species have been broadly classified as monomers or oligomers, based on comparisons with well-characterized reference species present in the aqueous phase. A similar methodology has allowed the study of changes occurring during calcination and activation steps of catalytic materials, but there are still uncertainties about their exact speciation.

This paper deals with the evaluation of superficial species of MoO_x over γ-Al_2O_3, H-ZY and H-ZSM-5 by means of a bandgap analysis (E_g) of deconvoluted diffuse reflectance UV–vis spectra. The assignment of the different Mo species was corroborated with theoretical DFT calculations on simplified zeolite clusters containing MoO_x species. A simplified kinetic network for the reactions occurring during the migration process is also proposed.

2. Experimental details

The materials used were γ-Al_2O_3 (Ketjen 0003P) and zeolites H-Y (UOP, Si/Al = 2.7) or H-ZSM-5 (Zeocat Pentasil PZ2754 Na Si/Al = 37). We heated physical mixtures of the supports with 5–15 wt% MoO_3 (99.5%, Aldrich) at 723 K for different lengths of time. The temperature used was above the MoO_3 Tammann temperature (534 K).

The samples were analysed by XRD (Siemens D500 x-ray diffractometer, Cu Kα radiation) and diffuse reflectance in the UV–vis region (Cary 5E). Diffuse reflectance spectra were transformed to Kubelka–Munk units. The bandgap analysis is described in a previous
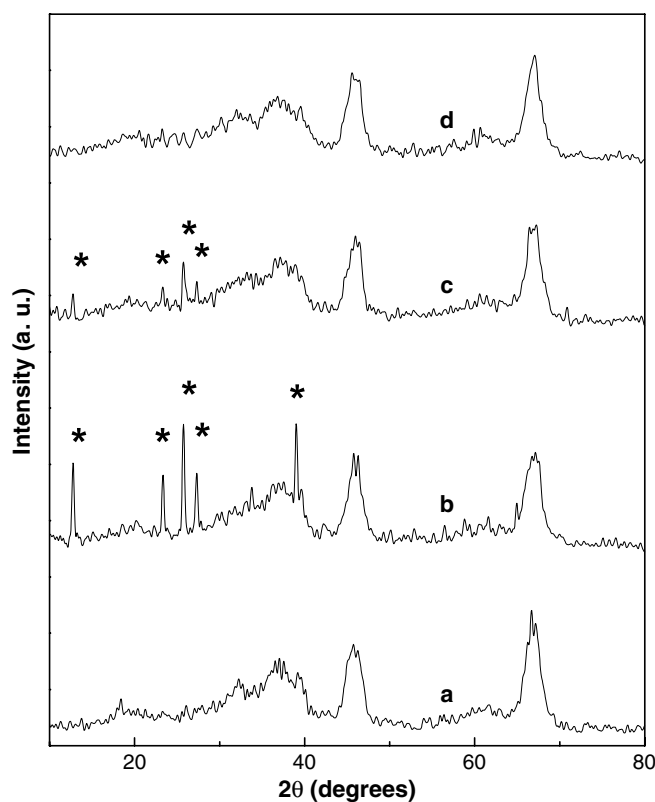
Figure 1. X-ray diffraction patterns of (a) pure γ-Al$_2$O$_3$; (b) physical mixtures of MoO$_3$ and γ-Al$_2$O$_3$ without thermal treatment; (c) heated for 1 h at 723 K; (d) heated for 24 h at 723 K. MoO$_3$ reflections are indicated by asterisks (∗).

paper [15]. Briefly, it is based on the deconvolution of the generally broad electronic spectra using Gaussians placed according to the bandgap energy of the different MoO$_x$ structures. The bandgap in these cases corresponds to the O $\rightarrow$ Mo charge transfer transition. We either determined the bandgap or made use of data in the literature [15].

In order to corroborate our assignments in the present study, gradient-corrected density functional theory (DFT) was used to determine the structure and stability of MoO$_x$ bound to a ZSM-5 simplified cluster. Gradient-corrected density functional theory was carried out using the B3LYP functional to estimate electron exchange and correlation contributions to the energy. The 6-31G* basis set was used to describe all atoms. In the case of Mo, pseudopotentials were calculated by using the Pulais DIIS approximation.

3. Results and discussion

During thermal treatments at 723 K, the structure of either alumina or the zeolites was preserved and MoO$_3$ was dispersed over the supports. This was shown by the disappearance of the MoO$_3$ signal in the XRD patterns of the samples. This suggests the formation and spreading of MoO$_x$ on all supports. However, the way MoO$_3$ spread was different on each support, i.e. it was affected by the porous structure of the support [14]. In the case of γ-Al$_2$O$_3$, MoO$_3$ was able to spread completely, see figure 1, in agreement with the results of Wang *et al* [16]. In the case of
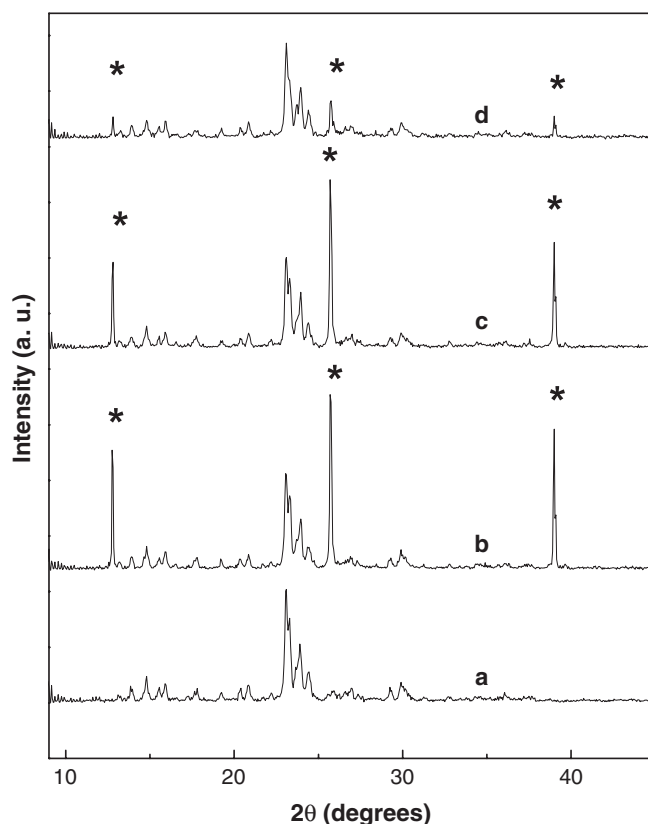
Figure 2. X-ray diffraction patterns of (a) pure H-ZSM-5; (b) physical mixtures of MoO$_3$ and H-ZSM-5 without thermal treatment; (c) heated for 1 h at 723 K; (d) heated for 24 h at 723 K. MoO$_3$ reflections are indicated by asterisks (∗).

zeolites, even after 24 h of thermal treatment MoO$_3$ was still detected based on several XRD peaks, although their intensities were smaller than those observed in the starting mixture before any thermal treatment. Figure 2 presents the spectra of MoO$_x$/ZSM-5. The decrease in XRD intensities of the MoO$_3$ reflections followed the sequence: γ-Al$_2$O$_3$ $\gg$ H-Y > H-ZSM-5.

Braun *et al* [17] reported the spreading of MoO$_3$ over SiO$_2$ and Al$_2$O$_3$ by thermal activation. They detected by XRD the disappearance of MoO$_3$ towards amorphous species and a large distortion of little clusters of Mo species by Raman spectroscopy. We did not detect by XRD any amorphous phase attributable to Mo species, as figures 1 and 2 show. Although in the case of Al$_2$O$_3$ the base spectrum presents broad absorption bands in the 20°–40° 2θ range, it is apparent that there are no significant absorption bands corresponding to MoO$_3$ after a prolonged heat treatment. In all cases, the width of MoO$_3$ reflections did not increase, and only their intensities decreased as a result of thermal treatments. This is shown by the variations in the $I(040)/I(060)$ ratio of the MoO$_3$ reflections. The disappearance of the XRD MoO$_3$ reflections in the case of γ-Al$_2$O$_3$ has been explained as a consequence of the formation of a monolayer or submonolayer of MoO$_x$ species covering the support surface, i.e. three-dimensional MoO$_3$ evolved to Mo bidimensional species [18]. XRD gives only information about the disappearance of MoO$_3$. It is necessary to use other techniques in order to determine what are the surface structures formed.
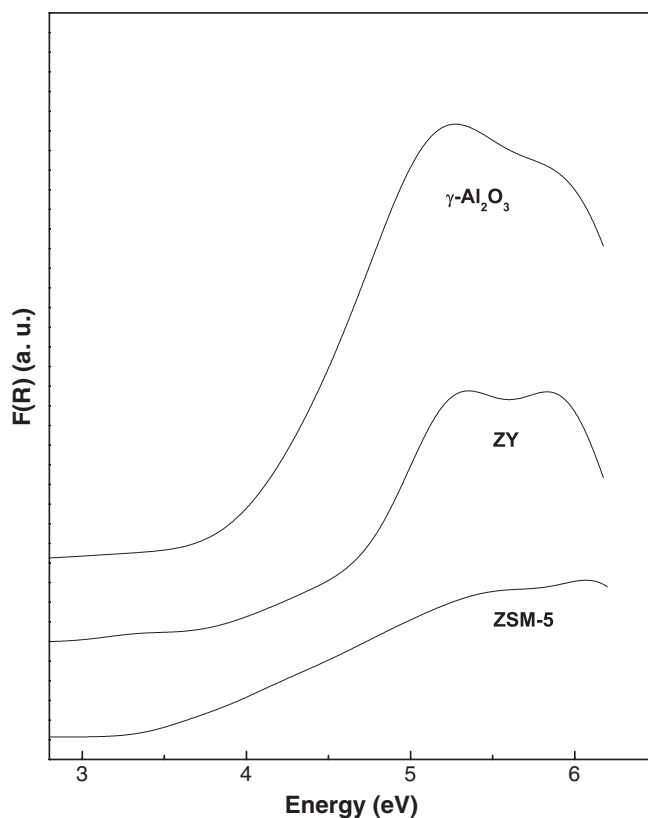
Figure 3. UV–vis diffuse reflectance spectra of samples prepared by heating physical mixtures of crystalline MoO$_3$/support at 723 K for 24 h.

We used UV–vis diffuse reflectance spectroscopy to study the dispersion process and the formation of Mo species over the supports as a result of thermal activation (figure 3). In agreement with the XRD results, UV–vis showed that the dispersion processes over alumina and over zeolites were different. Use of this technique also allowed us to determine the particular Mo surface species [14]. The intensities of UV–vis spectra varied as a result of changes in the particle size of MoO$_3$ crystals and the resulting transformation of MoO$_3$ into different MoO$_x$ surface species. Based on the bandgap analysis and the deconvolution of MoO$_x$/γ-Al$_2$O$_3$, MoO$_x$/H-Y and MoO$_x$/H-ZSM-5 spectra, we assigned four O^{2-} → Mo^{6+} charge transfer bands to species having either tetrahedral or octahedral coordination. The species corresponded to MoO$_3$ and moieties with structures equivalent to [MoO$_4$]$^{2-}$, [Mo$_2$O$_7$]$^{2-}$ and [Mo$_7$O$_{24}$]$^{6-}$ [14, 15].

To further validate our bandgap assignments we carried out DFT calculations of model structures. The simplified zeolite cluster containing Mo$_2$O$_7$ used for DFT calculations is shown in figure 4. This cluster was based on the distribution of Al in a silicon-rich zeolite such as ZSM-5. The stabilization of Mo dimers required the presence of two Al T sites as next-nearest neighbours (NNN). According to Rice *et al* [19], the fraction of Al T sites present as NNN is 0.27 for a ZSM-5 sample having the same Si/Al ratio as ours (Si/Al = 37). This means that it is possible to have a large population of dimers in ZSM-5 and supports our findings based on UV–vis.
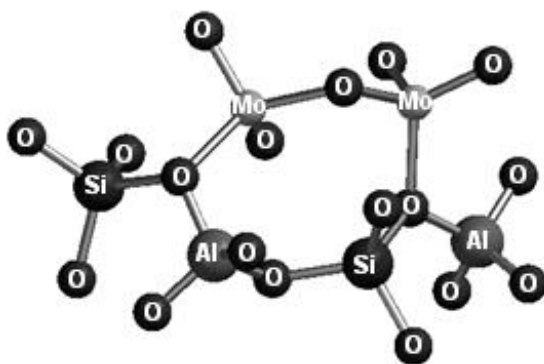
Figure 4. Theoretical DFT calculations on simplified zeolite clusters containing MoO_x species.
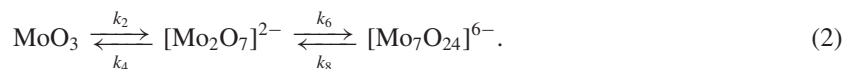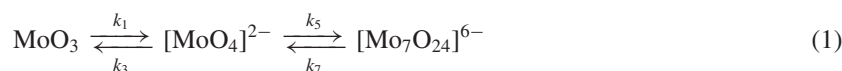
Table 1. Bandgap energy of Mo species estimated from the deconvolution of supported MoO_x spectra. The samples were heated at 723 K for 15 min.

Mo species	Band gap energy (eV)			
	γ-Al_2O_3	H-Y	ZSM-5	DFT[a]
MoO_3	2.72	2.78	3.33	—
$(MoO_4)^{2-}$	5.22	5.25	5.61	6.6
$(Mo_2O_7)^{2-}$	4.46	4.48	4.77	5.2
$(Mo_7O_{24})^{6-}$	3.59	3.58	3.71	3.8

[a] Based on DFT calculations on simplified ZSM-5 clusters similar to that presented in figure 4.

The HOMO–LUMO gaps calculated from DFT simulations were in good agreement with those determined from our analysis of the UV–vis spectra (table 1). The bond distances of our equilibrium structures were also in good agreement with those reported [20]. The DFT-calculated bond length Mo = O was ~1.7 Å whereas Mo–O–Mo and Mo–$O_{zeolite}$ bond lengths were longer, ~1.9–2.0 Å and ~2.10 Å, respectively. Central oxygen atoms could form very long bonds, ~2.30 Å, depending on the amount of oxygen atoms present.

The intensities of the different bands obtained from deconvolution of the full UV–vis spectra followed well-defined trends. Figure 5 shows those trends for MoO_x/H-ZSM-5. Although the intensities of the bands determined from diffuse reflectance experiments provide only a semi-quantitative measure of the oxospecies surface concentrations, if first-order kinetics are assumed it is possible to obtain a reasonable approximation of the kinetic scheme that underlies the dispersion process during thermal treatments. We analysed the data using a kinetic scheme given by equations (1) and (2):

$$MoO_3 \underset{k_3}{\overset{k_1}{\rightleftarrows}} [MoO_4]^{2-} \underset{k_7}{\overset{k_5}{\rightleftarrows}} [Mo_7O_{24}]^{6-} \tag{1}$$

$$MoO_3 \underset{k_4}{\overset{k_2}{\rightleftarrows}} [Mo_2O_7]^{2-} \underset{k_8}{\overset{k_6}{\rightleftarrows}} [Mo_7O_{24}]^{6-}. \tag{2}$$

The solution for the system MoO_x/H-ZSM-5 is shown in figure 6. There is competition between the formation of $[MoO_4]^{2-}$ and of $[Mo_2O_7]^{2-}$ starting from MoO_3. Both reactions are essentially irreversible ($k_3 = 0$ and $k_4 = 0$). However, on all supports the ratio k_1/k_2 was much larger than 1, i.e. there was a larger production of monomer. The kinetic analysis suggests that the heptamer is only formed from polymerization of $[MoO_4]^{2-}$ ($k_6 = 0$ and $k_8 = 0$) through a reversible reaction. It is important to mention that dispersion of MoO_x
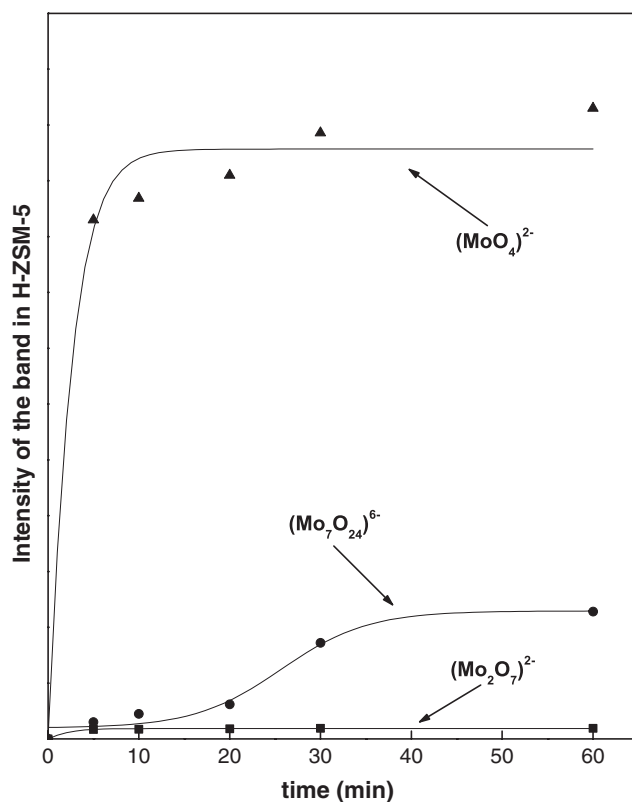
Figure 5. Intensity of the MoO$_x$ UV absorption bands as a function of time. Support: H-ZSM-5; $T = 723$ K.

species only happens in the presence of water, probably through the formation of MoO$_2$(OH)$_2$ over the support, although in this scheme this is not considered explicitly. Using an equilibrium step for the formation of the hydrated intermediate leads to global kinetic equations equivalent to equations (1) and (2).

The results demonstrate the complexity of the migration process and the redistribution of the MoO$_x$ species on the different supports. It is clear that the structural characteristics of the support, i.e. pore diameter, Si/Al ratio and concentration of –OH groups, limit the MoO$_x$ structures that migrate and hence their catalytic activity. The bandgap analysis used to deconvolute UV–vis spectra allows us to determine the presence of tetrahedral and octahedral MoO$_x$ species on the supports, but also gives us the possibility of doing kinetic analysis and extracting further information about the mechanism underlying the thermally activated migration of MoO$_x$ moieties. It is worthwhile mentioning that our bandgap assignments are also supported on DFT calculations of model clusters that match closely the experimental observations. We are pursuing these analyses further.

4. Conclusions

- The principal species determined from bandgap analysis were [MoO$_4$]$^{2-}$, [Mo$_2$O$_7$]$^{2-}$ and [Mo$_7$O$_{24}$]$^{6-}$, as well as MoO$_3$ crystals.
- The type and concentration of MoO$_x$ species in the different supports is a function of their Si/Al ratio and apparently of their porous structure.
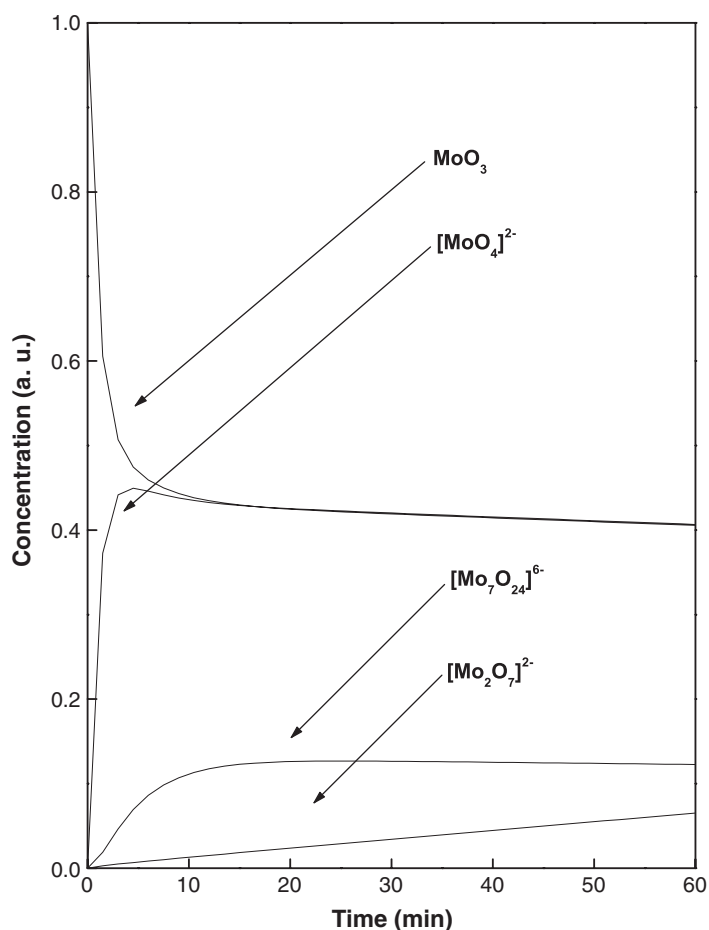
Figure 6. Time-dependent variation of the concentration of MoO_3 and of surface molybdenum oxospecies on H-ZSM-5 after the solution of equations (1) and (2).

- The spreading of MoO_x species over H-Y and H-ZSM-5 zeolites is observed to favour formation of tetrahedral species, i.e. monomers resembling $[MoO_4]^{2-}$ and dimers like $[Mo_2O_7]^2$, seemingly because of a molecular sieve effect. Al_2O_3 has no size restriction and species equivalent to $[Mo_7O_{24}]^{6-}$ are formed preferentially.
- Bond distances and energies for MoO_x species calculated by DFT on model clusters were found to be in good agreement with those measured experimentally.
- Kinetics of the migration of MoO_3 are consistent with the reaction scheme:

$$MoO_3 \longrightarrow [MoO_4]^{2-} \longrightarrow [Mo_7O_{24}]^{6-}$$

$$MoO_3 \longrightarrow [Mo_2O_7]^{2-}.$$
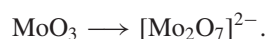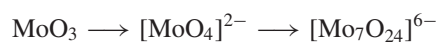
References

[1] Ono Y and Kanae K 1991 *J. Chem. Soc. Faraday Trans.* **87** 663
[2] Guisnet M, Gnep N S and Alario F 1992 *Appl. Catal.* **89** 1
[3] Gnep N S, Doyemet J Y and Guisnet M 1988 *J. Mol. Catal.* **45** 281

[4] De Bont P W, Vissenberg M J, De Beer H H J, Van Veen J A R, Van Santen R A and van der Kraan A M 2000 *Appl. Catal.* A **202** 99
[5] Kucherov A V and Slinkin A A 1987 *Zeolites* **7** 43
[6] Moorehead E L 1981 *US Patent* 4 297 243
[7] Ward M B and Lunsford J H 1984 *Proc. 6th Int. Conf. on Zeolite 1983* ed D H Olson and A Bisio (London: Butterworths) p 405
[8] Johns J R and Howe R F 1985 *Zeolites* **5** 251
[9] Abdo S and Howe R F 1983 *J. Phys. Chem.* **87** 1713
[10] Okamoto Y and Katsuyama H 1996 *Ind. Eng. Chem. Res.* **35** 1834
[11] Chen L Y and Hsu T C 1971 *J. Chin. Inst. Chem. Eng.* **2** 25
[12] Howe R F, Ming J, Wong S-T and Zhu J-H 1989 *Catal. Today* **6** 113
[13] Borry R W III, Kim Y H, Huffsmith A, Reimer J A and Iglesia E 1999 *J. Phys. Chem.* B **103** 5787
[14] Mosqueira L and Fuentes G A 2002 *Mol. Phys.* **100** 3055
[15] Weber R S 1995 *J. Catal.* **151** 470
[16] Wang L, Tao L, Xie M and Xu G 1993 *Catal. Lett.* **21** 35
[17] Braun S, Appel L G, Camorim V L and Schmal M 2000 *J. Phys. Chem.* B **104** 6584
[18] Xie Y, Gui L, Liu Y, Zhang Y, Zhao B, Yang N, Guo Q, Duan L, Huang H, Cai X and Tang Y 1985 *Adsorption and Catalysis on Oxide Surfaces* ed M Che and G C Bond (Amsterdam: Elsevier) p 139
[19] Rice M J, Chakraborty A K and Bell A 1999 *J. Catal.* **186** 222
[20] Cotton F A, Wilkinson G, Murillo C A and Bochmann M 1999 *Advanced Inorganic Chemistry* 6th edn (New York: Wiley)